Available online at www.sciencedirect.com
SCIENCE DIRECT®
Journal of Sound and Vibration 277 (2004) 741–763
JOURNAL OF SOUND AND VIBRATION
www.elsevier.com/locate/jsvi

Vibration and sound radiation of sandwich beams with honeycomb truss core

M. Ruzzene*

School of Aerospace Engineering, Georgia Institute of Technology, 270 Ferst Drive, Atlanta, GA 30332–0150, USA

Received 3 April 2003; accepted 8 September 2003

Abstract

The vibrations of and the sound radiation from sandwich beams with truss core are analyzed. The structure of the core is composed of a sequence of identical unit cells repeating along the beam length and across the core thickness. Each cell is composed of beam elements assembled to form a frame structure. Layouts with the typical honeycomb pattern arranged through the thickness of the core are here considered. This design represents an alternative with respect to the traditional application of honeycombs in sandwich construction. The proposed configuration provides sandwich beams with interesting structural as well as acoustic characteristics.

A finite element model is developed to evaluate the structural and the acoustic behavior of the considered class of sandwich beams. The model is formulated by employing dynamic shape functions, derived directly from the distributed parameter model of beam elements. This formulation, often denoted as "spectral", allows an accurate evaluation of the dynamic behavior of the considered structures at high frequencies and with a limited number of elements. In addition, the spectral model can be easily coupled with a Fourier transform based analysis of the sound radiated by the fluid-loaded structure.

The model is used to analyze the performance of beams with various core configurations. The comparison is carried out in terms of structural response and sound transmission reduction index. In addition the sound pressure levels and distributions resulting from the beam vibration in an unbounded acoustic half-plane are evaluated and compared. Hexagonal and re-entrant configurations are considered in an effort to study the effects of core geometry on structural response and acoustic radiation.

*Tel.: +1-404-894-3078; fax: +1-404-894-2760.
E-mail address: massimo.ruzzene@aerospace.gatech.edu (M. Ruzzene).

0022-460X/$ - see front matter © 2003 Elsevier Ltd. All rights reserved.
doi:10.1016/j.jsv.2003.09.026

1. Introduction

The multifunctional properties of cellular solids have generated great interest for their application in ultra-light structures. The properties that appear most attractive are those that govern the use of cellular solids as cores for panels and shells having lower weight than competing materials, and potentially superior heat dissipation, vibration control and energy dissipation characteristics [1–3]. Commercially available cellular solids and foams have random microstructures and their properties have been thoroughly documented (see for example Refs. [1,3]). An interesting research trend in cellular materials consists of the study and the application of deterministic periodic architectures, whose topology can be designed and tailored for the considered component to achieve performances greatly superior than those demonstrated by their stochastic analogues [3]. The scalable geometry of deterministic periodic architectures, whereby the structural properties depend on the actual size of the unit cells, allows for their application to both small-scale and large-scale structural systems. Examples of applications of deterministic periodic cellular architectures include the lattice material and prismatic core concepts [2,5]. Both configurations have been employed and studied in the past as alternative core configurations for sandwich structures with superior structural characteristics and potential multifunctional capabilities. For example, the application of the lattice material concept has lead to the design of truss core sandwich constructions, whose optimized structural performance has proven to be competitive with traditional sandwich honeycomb and stiffened structures [5].

In this paper, the dynamic response and the sound radiation of truss core sandwich beams is investigated. The structural-acoustic performance of periodic truss core panels has been investigated by El-Raheb, who in Ref. [6] studied the frequency response of two-dimensional panels using the transfer matrix method, and in reference [7] presented an interesting hybrid technique to predict their elasto-acoustic behavior. In his work, El-Raheb focused on the analysis of the performance of panels with a given configuration and evaluated the effect on the response of a number of parameters, such as fluid-loading and damping. The research has then been extended to evaluate the behavior of double truss-like panel and to discuss the phenomenon of the disappearance for this configuration, of the mass–spring–mass resonance and its dependence on panel aspect ratio [8].

This paper analyzes the performance of sandwich beams with truss core elements arranged according to honeycomb configurations. In the proposed design, the hexagonal topology is developed across the thickness of the sandwich structure, as opposed to the layout of conventional honeycomb sandwich constructions. The proposed sandwich beams hence can be more appropriately described as examples of applications of prismatic materials as defined in Ref. [2], and the "truss core" terminology used throughout the paper should be considered as having a wider meaning. The proposed honeycomb configurations are an alternative to the truss-like panels presented in Refs. [6–8]. The core results from the assembly of unit cells, whose shape and geometry are defined by the cell aspect ratio and by an internal angle. Focus is placed in the analysis of the performance of cores with re-entrant geometries as described in Refs. [1,9]. Re-entrant cellular architectures have been widely studied in the past as viable alternatives for the design of honeycomb cores with superior shear modulus and compressive strength [10,11]. Re-entrant two-dimensional cellular structures have also shown unique beaming characteristics,

whereby the propagation of elastic waves at given frequencies is restricted to specified directions [12].

The dynamic behavior of the considered sandwich beams is predicted by a finite element model, which employs shape functions derived directly from the solution of distributed parameter models for each beam element. This formulation, often denoted as "spectral" [13–15], accurately describes the dynamic response of the structure with a reduced number of elements. The considered dynamic shape functions are in fact able to capture the response of each element for given nodal displacements, even for high excitation frequencies. The developed model also allows capturing local phenomena, such as for example the resonance of the core elements, that help understanding the fundamentals of operation of the considered structures and provide important guidelines for their design. In addition, the spectral formulation can be easily and efficiently coupled with the Fourier transform (FT) based analysis of the structure's sound radiation in a surrounding acoustic medium. Hence the proposed formulation is an efficient numerical tool for the analysis of the dynamic and acoustic performance of the considered truss core sandwich beams.

The paper is organized in 6 sections. In Section 1 a brief introduction is given. Section 2 describes the configuration considered for the truss core beams and the goals of this study. The spectral formulation for the dynamic response of the beam is presented in Section 3, while the procedure for the analysis of sound radiation from the structure is outlined in Section 4. The structural and acoustic performance of the considered beams is described in Section 5. Finally, Section 6 summarizes the main results of the study and provides recommendations for future work.

2. Concept and considered configuration

The considered sandwich beam features a truss-type core with elements arranged according to a honeycomb configuration. The honeycomb geometry is laid out across the thickness of the core, as depicted in Fig. 1. The core is obtained by the assembly of identical cells, which are replicated along the length of the beam and across the thickness of the core. The cell geometry is defined by its dimensions L_x and L_y and by the internal angle θ. For example, an internal angle $\theta = 30^\circ$ and a cell aspect ratio $L_x/L_y = \sqrt{3}$ define a regular hexagonal configuration (Fig. 1(a)). Several configurations for the core can be obtained by modifying the aspect ratio or the internal angle. For assigned beam length and core thickness, the aspect ratio determines the number of cells across the thickness and along the length of the beam, while the internal angle defines the cell shape. The beams depicted in Fig. 1 both have a core composed of 2 cells across the thickness and 10 cells along the beam length. The performance of cores defined by positive (counterclockwise) (Fig. 1(a)) and negative (clockwise) internal angles (Fig. 1(b)) are here considered. The vibro-acoustic behavior of this class of sandwich beams is compared with that of truss core beams of the kind studied in Refs. [6,7] and schematically depicted in Fig. 2. In this paper, the core depicted in Fig. 2 will be denoted as "square", as opposed to the hexagonal cores shown in Fig. 1.

In the considered configuration (Fig. 3), the beam is part of a rigid baffle of infinite length. The bottom layer is excited by a plane incident pressure wave varying harmonically in time, while the top layer faces an unbounded half-plane fluid domain. The vibration of the bottom layer induced

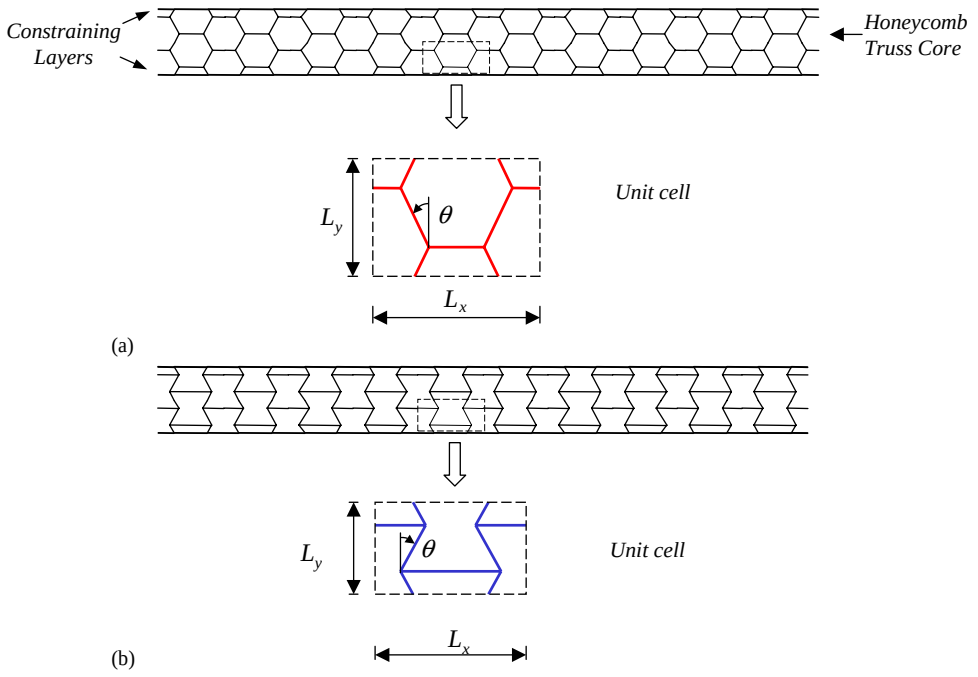

Fig. 1. Schematic of beams with hexagonal core: (a) honeycomb-type, and (b) re-entrant configuration.

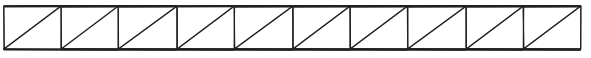

Fig. 2. Truss core beam with "square" core.

by the incident pressure wave is transmitted through the core to the top layer, which radiates sound in the fluid domain.

3. Vibration of beams with truss core: spectral finite element modelling

The considered sandwich beam is composed of rigidly connected beam elements, and thus is modelled as a frame structure. The elements are oriented in the plane of the structure xy according to the core topology. The dynamic behavior of each element is described in the local reference system $\xi\psi$, rotated with respect to the global reference system xy of the angle φ (see Fig. 4).

3.1. Distributed parameter model in the local reference system

The equations of motion and boundary conditions governing the longitudinal and transverse vibrations of a beam element can be derived by applying Hamilton's principle:

$$\int_{t_1}^{t_2} \delta(T - U + W)\,\mathrm{d}t = 0, \tag{1}$$

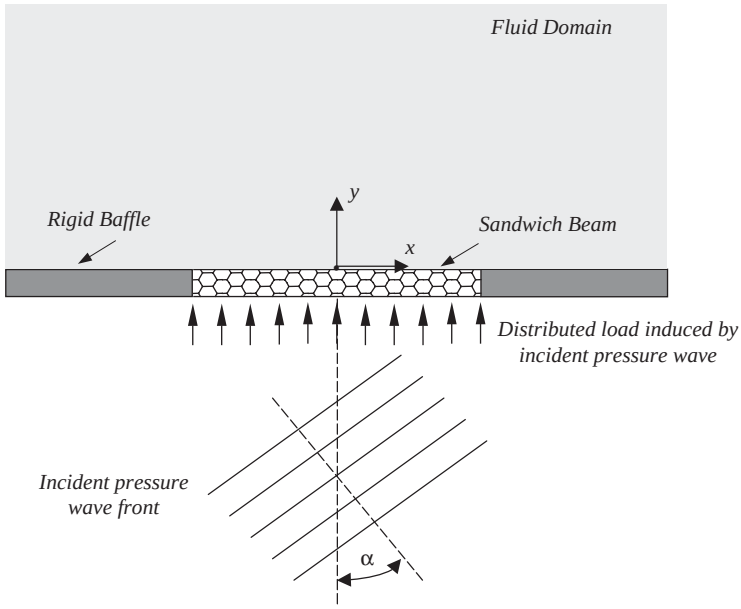

Fig. 3. Considered loading and radiation condition for the baffled sandwich beam.

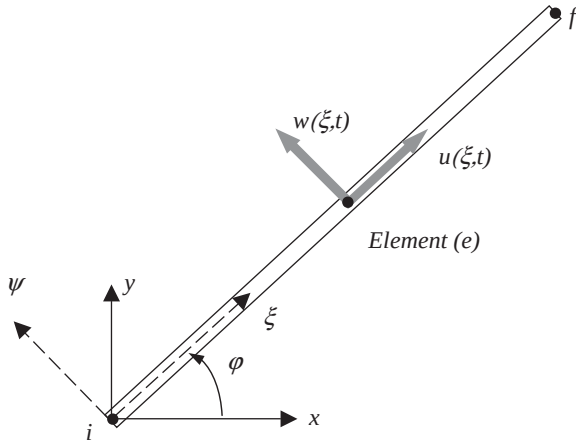

Fig. 4. Global and local reference systems and element degrees of freedom.

where $\delta(.)$ denotes the first variation, t_1 and t_2 are the initial and final time, T and U are respectively the kinetic and the strain energy of the beam, and W is the work of the external forces. Each element is considered as an Euler–Bernoulli beam, and includes also axial degrees of freedom. Accordingly, in the local reference system, the beam's strain and kinetic energies are

given by

$$U = \tfrac{1}{2}EA \int_0^L u_\xi^2(\xi, t)\,\mathrm{d}\xi + \tfrac{1}{2}EI \int_0^L w_{\xi\xi}^2(\xi, t)\,\mathrm{d}\xi, \tag{2}$$

$$T = \tfrac{1}{2}m \int_0^L \dot{u}_t^2(\xi, t) + \dot{w}_t^2(\xi, t)\,\mathrm{d}\xi, \tag{3}$$

where E is the Young's Modulus of the beam material, A, I are respectively the area and the second moment of area of the beam cross-section, and m is the mass per unit length of the beam. Subscripts ξ and t in Eqs. (2) and (3), respectively, denote partial differentiation with respect to the longitudinal co-ordinate ξ and time t. Also, in Eqs. (2) and (3) u and w are the axial and the transverse displacement of the beam.

The work of the external forces can be expressed as

$$W = \int_0^L u(\xi, t) q_u(\xi, t)\,\mathrm{d}\xi + \int_0^L w(\xi, t) q_w(\xi, t)\,\mathrm{d}\xi, \tag{4}$$

where $q_u(\xi, t), q_w(\xi, t)$ are externally applied distributed longitudinal and transverse loads per unit length.

Substituting U, T and W in Eq. (1) and performing the variations gives the following set of partial differential equations of motion describing the beam's longitudinal and transverse vibration:

$$\begin{aligned} &Ku_{\xi\xi}(\xi, t) - mu_{tt}(\xi, t) = -q_u(\xi, t), \\ &Dw_{\xi\xi\xi\xi}(\xi, t) + mw_{tt}(\xi, t) = -q_w(\xi, t), \end{aligned} \tag{5}$$

where $K = EA$ and $D = EI$ are the beam's longitudinal and flexural rigidities.

For harmonic motion at frequency ω, Eq. (5) reduce to ordinary differential equations, and can be rewritten as

$$\begin{aligned} &Ku_{\xi\xi}(\xi, \omega) + \omega^2 mu(\xi, \omega) = -q_u(\xi, \omega), \\ &Dw_{\xi\xi\xi\xi}(\xi, \omega) - \omega^2 mw(\xi, \omega) = -q_w(\xi, \omega). \end{aligned} \tag{6}$$

3.2. Degrees of freedom and shape functions

The homogeneous solution for Eq. (6) can be found in the form

$$\begin{aligned} u(\xi, \omega) &= a_1 \mathrm{e}^{k_a \xi} + a_2 \mathrm{e}^{-k_a \xi}, \\ w(\xi, \omega) &= a_3 \mathrm{e}^{k_{b1} \cdot \xi} + a_4 \mathrm{e}^{-k_{b1} \cdot \xi} + a_5 \mathrm{e}^{k_{b2} \cdot \xi} + a_6 \mathrm{e}^{-k_{b2} \xi}, \end{aligned} \tag{7}$$

where a_i $(i = 1, \ldots, 6)$ are integration constants, and

$$k_a = \left(\omega^2 \frac{m}{K}\right)^{1/2}, \quad k_{b1} = \left(\omega^2 \frac{m}{D}\right)^{1/4}, \quad k_{b2} = \mathrm{i}\left(\omega^2 \frac{m}{D}\right)^{1/4} \tag{8}$$

are the wavenumbers of longitudinal and transverse elastic waves.

The beam's behavior is described by the following vector of nodal degrees of freedom:

$$\{\delta^{(e)}\} = \{\, u_i \quad w_i \quad w_{\xi i} \quad u_f \quad w_f \quad w_{\xi f} \,\}^{\mathrm{T}}, \tag{9}$$

where i and f denote the initial and final node of the considered beam element (see Fig. 4), and where $w_\xi = \partial w/\partial \xi$ is the slope of the cross-section at the considered location. Imposing the displacements at the element boundaries in Eq. (7) expresses the coefficients a_i in terms of $\{\delta^{(e)}\}$, which finally yields:

$$\left\{ \begin{array}{c} u(\xi,\omega) \\ w(\xi,\omega) \end{array} \right\} = [N(\xi,\omega)] \cdot \{\delta^{(e)}(\omega)\}, \tag{10}$$

where $[N(\xi,\omega)]$ is the matrix of shape functions, which are obtained from the solution of the beam's distributed parameter model for harmonic motion at frequency ω. Within the validity of Euler–Bernoulli assumptions, these shape functions reproduce the exact displacement of the considered beam element for the assigned set of nodal displacements. Accordingly, a single finite element is sufficient to fully characterize the response of the beam for any value of frequency ω. This finite element formulation, often denoted as "spectral" [13–15], allows an accurate prediction of the dynamic response of the global structure by using a reduced number of elements. The spectral formulation for rod and beam elements can be found in Ref. [13], where a Timoshenko beam element is also given. The model presented here combines the rod and beam formulations given in reference [13]. The Euler–Bernoulli assumption is considered given the geometry of the beams (see Section 5). As opposed to traditional finite element formulations, the number of elements does not need to be increased to fully capture the dynamic response at high frequencies. One should however note that the evaluation of the shape functions from the continuous beam model requires the inversion of a matrix containing exponentials defined in terms of the wave numbers and the beam's geometry. For extremely high frequencies such an inversion may become affected by numerical errors that limit the accuracy of the analysis. These numerical difficulties can be circumvented by reducing the elements' length, thus considering finer meshes. Regardless of such limitations, the high-frequency behavior can be captured with a substantially reduced number of elements with respect to conventional finite element formulations. Finally, the spectral formulation can be easily modified to include the effects of the interaction of the vibrating structure with a surrounding fluid medium. In particular, the spectral model nicely ties in with a FT based analysis of the beam sound radiation in the surrounding acoustic domain. The fluid–structure interaction formulation for the considered configuration will be described in Section 4.

3.3. Spectral mass and stiffness matrices and load vector

Substituting Eq. (10) in the expressions of the strain and kinetic energy for the considered beam element gives

$$U^{(e)}(\omega) = \tfrac{1}{2}\{\delta^{(e)}(\omega)\}^{\mathrm{T}}[K^{(e)}(\omega)]\{\delta^{(e)}(\omega)\}, \tag{11}$$

$$T^{(e)}(\omega) = -\frac{\omega^2}{2}\{\delta^{(e)}(\omega)\}^{\mathrm{T}}[M^{(e)}(\omega)]\{\delta^{(e)}(\omega)\}, \tag{12}$$

where $\lfloor K^{(e)}(\omega) \rfloor$ and $\lfloor M^{(e)}(\omega) \rfloor$ are respectively the beam stiffness and mass spectral matrices, obtained in the local reference system and at the given frequency ω.

Similarly, the work of the external loads can be expressed as

$$W^{(e)}(\omega) = \{f^{(e)}(\omega)\}^{\mathrm{T}}\{\delta^{(e)}(\omega)\}, \tag{13}$$

where $\{f^{(e)}(\omega)\}$ is the load vector.

3.4. Equation of motion in the global reference system

The components of the beam longitudinal and transverse displacements u, w with respect to the global reference system xy are given in terms of the rotation angle φ in Fig. 4. Accordingly the vector of nodal displacements in the global reference system $\{\Delta^{(e)}(\omega)\}$ is related to the local nodal displacements vector $\{\delta^{(e)}(\omega)\}$ through a rotation matrix $[R]$:

$$\{\delta^{(e)}(\omega)\} = [R] \cdot \{\Delta^{(e)}(\omega)\}, \tag{14}$$

where $[R]$ is defined in terms of the angle φ. Substituting Eq. (14) in the expression of the strain and kinetic energy gives

$$U^{(e)}(\omega) = \tfrac{1}{2}\{\Delta^{(e)}(\omega)\}^{\mathrm{T}}[K_r^{(e)}(\omega)]\{\Delta^{(e)}(\omega)\}, \tag{15}$$

$$T^{(e)}(\omega) = -\frac{\omega^2}{2}\{\Delta^{(e)}(\omega)\}^{\mathrm{T}}[M_r^{(e)}(\omega)]\{\Delta^{(e)}(\omega)\}, \tag{16}$$

where $\left[K_r^{(e)}(\omega)\right] = [R]^{\mathrm{T}} \cdot [K^{(e)}(\omega)] \cdot [R]$ and $\left[M_r^{(e)}(\omega)\right] = [R]^{\mathrm{T}} \cdot [M^{(e)}(\omega)] \cdot [R]$ are the mass and stiffness spectral matrices in the xy reference system.

Similarly, the work of the external forces can be rewritten as

$$W^{(e)}(\omega) = \{F^{(e)}(\omega)\}^{\mathrm{T}}\{\Delta^{(e)}(\omega)\}, \tag{17}$$

where $\{F_r^{(e)}(\omega)\} = [R]^{\mathrm{T}} \cdot \{f^{(e)}(\omega)\}$ is the load vector in the global reference system.

The spectral formulation described above considers the dynamic problem associated with the beam's vibration at frequency ω, as a static equilibrium problem [13,14]. A spectral energy functional for element (e) can be defined as

$$\Pi^{(e)}(\omega) = U^{(e)}(\omega) + T^{(e)}(\omega) - W^{(e)}(\omega). \tag{18}$$

The spectral potential energy for the whole sandwich beam structure is given by

$$\begin{aligned}\Pi(\omega) &= U(\omega) + T(\omega) - W(\omega),\\ \Pi(\omega) &= \tfrac{1}{2}\{\Delta(\omega)\}^{\mathrm{T}}([K(\omega)] - \omega^2[M(\omega)])\{\Delta^{(e)}(\omega)\} - \{F(\omega)\}^{\mathrm{T}}\{\Delta^{(e)}(\omega)\},\end{aligned} \tag{19}$$

where $[K(\omega)], [M(\omega)], \{F(\omega)\}$ are the structure's mass and stiffness matrices and global load vector, obtained from the element matrices and vector through standard assembly procedures. Minimizing the energy functional yields the following spectral equation of motion for the sandwich beam:

$$([K(\omega)] - \omega^2[M(\omega)])\{\Delta(\omega)\} = \{F(\omega)\}. \tag{20}$$

Solution of Eq. (20) for an assigned frequency ω gives the amplitude of the displacements at each node. The displacements within each element can be then obtained through the shape functions described by Eq. (10).

4. Sound radiation in the acoustic domain

The configuration for the sandwich beam is depicted in Fig. 3. The bottom layer is excited by a plane pressure incident wave, which varies harmonically in time and can be expressed as

$$p_i(x, y, t) = p_i(x, y, \omega)\mathrm{e}^{-\mathrm{i}\omega t}, \tag{21}$$

where

$$p_i(x, y, \omega) = p_{io}\mathrm{e}^{\mathrm{i}k_x x + \mathrm{i}k_y y} = p_{io}\mathrm{e}^{\mathrm{i}k(x\sin\alpha + y\cos\alpha)}. \tag{22}$$

In Eq. (22), p_{io} is the amplitude of the incident pressure, α is the angle of incidence measured with respect to the y-axis, and $k = \omega/c_a$ is the acoustic wave number, with c_a denoting the speed of sound in air.

4.1. Spectral load vector equivalent to the incident pressure

Each element belonging to the bottom layer is loaded by an incident pressure wave expressed by Eq. (21). The work of the corresponding distributed load at frequency ω is given by

$$W^{(e)}(\omega) = \int_0^{L^{(e)}} w_b(\xi, t) p_i(\xi, y_b, \omega) b \, \mathrm{d}\xi, \tag{23}$$

where y_b defines the location of the elements of the bottom layer in the global reference system, b is the beam off-plane width, $L^{(e)}$ is the element length, and w_b is the transverse displacement of the bottom layer. The local longitudinal co-ordinate ξ for the elements of the bottom layer is aligned with the global x-axis (see Fig. 3). Imposing the shape functions defined in Eq. (10) gives

$$\begin{aligned} W^{(e)}(\omega) &= \int_0^{L^{(e)}} (p_i(x, 0, \omega) \cdot [N(\xi, \omega)] b \, \mathrm{d}\xi) \cdot \{\delta^{(e)}(\omega)\} \\ &= \{f^{(e)}(\omega)\}^{\mathrm{T}} \{\delta^{(e)}(\omega)\}, \end{aligned} \tag{24}$$

where $\{f^{(e)}(\omega)\}$ is the spectral element load vector equivalent to the applied pressure distribution.

4.2. Sound radiation in the fluid domain: Fourier transform solution

The pressure distribution in the acoustic fluid domain facing the top layer of the beam can be obtained from the solution of Helmholtz equation [16]:

$$\left(\frac{\partial^2}{\partial x^2} + \frac{\partial^2}{\partial y^2} + k^2\right) p_t(x, y, \omega) = 0 \tag{25}$$

with the following boundary conditions:

$$\left.\frac{\partial p_t(x, y, \omega)}{\partial y}\right|_{y=0} = \rho_f \omega^2 w_t(x, \omega), \tag{26}$$

where ρ_f is the density of the fluid, $p_t(x, y, \omega)$ is the pressure radiated in the fluid, and $w_t(x, \omega)$ is the transverse displacement of the top layer (Fig. 3).

A solution for Eq. (25) can be conveniently found by considering the FT of Helmholtz equation with respect to the co-ordinate x, which gives [16]

$$\left(\frac{\partial^2}{\partial y^2} + k^2 - \gamma_x^2\right)\hat{p}_t(\gamma_x, y, \omega) = 0. \tag{27}$$

The FT of the pressure $\hat{p}_t(\gamma_x, y, \omega)$ must satisfy the transformed boundary conditions

$$\left.\frac{\partial \hat{p}_t(\gamma_x, y, \omega)}{\partial y}\right|_{y=0} = \rho_f \omega^2 \hat{w}_t(\gamma_x, \omega), \tag{28}$$

where $\hat{w}_t(\gamma_x, \omega)$ is FT of the top layer's transverse displacement, given by

$$\hat{w}_t(\gamma_x, \omega) = \int_{-L/2}^{L/2} w_t(x, \omega) \mathrm{e}^{-\mathrm{i}\gamma_x x}\, \mathrm{d}x. \tag{29}$$

In Eq. (29), the integration is limited to the length of the beam L, as the baffle is considered to be infinitely rigid and not undergoing any transverse motion (see Fig. 3).

The solution of Eq. (27) with boundary conditions expressed by Eq. (28) is given by

$$\hat{p}_t(\gamma_x, y, \omega) = -\mathrm{i}\rho_f \omega^2 \hat{w}_t(\gamma_x, \omega) \frac{\mathrm{e}^{\mathrm{i}y\sqrt{k^2-\gamma_x^2}}}{\sqrt{k^2 - \gamma_x^2}}. \tag{30}$$

The pressure distribution in the fluid domain is then obtained through the Inverse Fourier transform of Eq. (30).

4.3. Evaluation of transform solution through the spectral formulation

The spectral formulation presented in Section 3 allows an easy application and numerical implementation of the Fourier transform solution for the radiated pressure. Discretizing the structure into finite elements and using dynamic shape functions such as those defined in Eq. (10) makes the evaluation of the displacement transform particularly simple. The integral over the finite length of the beam in Eq. (29) can be in fact evaluated as the sum of integrals over each element of the top layer, which can be expressed as

$$\hat{w}_t(\gamma_x, \omega) = \sum_{k=1}^{N_t} \int_0^{L^{(k)}} w_t(\xi, \omega) \mathrm{e}^{-\mathrm{i}\gamma_x(\xi - L^{(k)}/2)}\, \mathrm{d}\xi, \tag{31}$$

where N_t is the number of elements belonging to the top layer and where $L^{(k)}$ is the length of the kth element. Imposing the shape functions defined in Eq. (10) gives an expression for the displacement transform in terms of the vector of element nodal degrees of freedom $\{\delta^{(k)}\}$:

$$\hat{w}_t(\gamma_x, \omega) = \sum_{k=1}^{N_t} \int_0^{L^{(k)}} [N(\xi, \omega)] \mathrm{e}^{-\mathrm{i}\gamma_x(\xi - L^{(k)}/2)}\, \mathrm{d}\xi \{\delta^{(k)}\}. \tag{32}$$

The exponential form of the considered shape functions allows the analytical evaluation of the integrals in Eq. (32), which results in the exact evaluation of the displacement transform for given γ_x and frequency ω. The pressure distribution can be then determined through the numerical

estimation of the inverse pressure transform, according to the relation

$$p_t(x,y,\omega) \cong \frac{-i\rho_f\omega^2}{2\pi}\sum_{-n}^{n}\hat{w}_t(n\Delta\gamma_x,\omega)\frac{e^{iy\sqrt{k^2-(n\Delta\gamma_x)^2}}}{\sqrt{k^2-(n\Delta\gamma_x)^2}}e^{in\Delta\gamma_x x}\Delta\gamma_x. \tag{33}$$

The analytical estimation of the displacement coefficients in Eq. (32) reduces the approximation introduced by the numerical evaluation of the pressure distribution.

5. Performance of beams with honeycomb truss core

5.1. Overview

The spectral formulation and the analysis of the sound radiation in the unbounded fluid medium are applied to evaluate the vibro-acoustic performance of beams with honeycomb truss core. Several configurations for the core can be considered to estimate the effect of its core geometry and configuration on the performance of the beam. The various configurations can be obtained by varying the cell aspect ratio and internal angle. Focus is here placed in the comparison of hexagonal and re-entrant lay-outs with more classical square core configurations. Simulations are performed for θ varying between -30° and 30° and for cores composed of 20 cells along the beam length and 1 cell across the core thickness. The evaluation of the influence of a varying number of cells in the core will be the object of future investigations. The performance analysis is carried out in terms of structural dynamic response, sound transmission loss, and radiated pressure in the fluid domain. In the following, the structural response of square core beams will be first analyzed, and comparisons with existing results will facilitate the interpretation of the findings for hexagonal core beams presented in Section 5.3. A discussion of the sound radiation characteristics for the two classes of beams will then conclude this section.

5.2. Structural response of square core beams

5.2.1. Geometry and material properties

The square core beams considered in the simulations are 2 m long and have a 5 cm thick core. Both layers and core elements are made of aluminum (Young's modulus 7.1e10, density 2700 kg/m^3), and have rectangular cross-sections. The same material is considered for the constraining layers and for the core, which is a common configuration for prismatic core beams [4–6]. The top and bottom layers are 5 mm thick, while the thickness of the elements of the core is 2.5 mm. The out-of-plane thickness of the structure b is constant for every element and set equal to unity for simplicity. Damping is introduced by considering a complex modulus for all the elements ($E = E^*(1 + i\eta)$), with a loss factor $\eta = 0.01$. This loss factor is higher than the values typically considered for aluminum ($\approx$10e–4), but has been here selected to include damping effects arising from the connection of the single beam elements. Such additional damping effect has been observed for example in metallic foams of open cell type [3]. In all the simulations the beams are connected to the rigid baffle by pin joints, thus simulating simply supported boundary conditions.

The performance of the beam is evaluated in the frequency range between 0 and 5000 Hz, which is relevant for most acoustic applications.

5.2.2. Beam response

The bottom layer of the beam is excited by a normally incident pressure wave of unit amplitude, according to the configuration depicted in Fig. 3. The response of the top and bottom layers is evaluated in terms of root mean square of the velocity along the y direction, which is related to the energy of transverse motion of the panel and the associated radiated sound [6,7]. The root mean square velocity for the bottom layer is calculated as

$$v_{r.m.s.}(\omega) = \left[\frac{1}{L}\int_0^L (\omega w_t(\xi,\omega))^2 \,\mathrm{d}\xi\right]^{1/2}, \tag{34}$$

where w_t is the transverse displacement of the top layer. The root-mean square velocity is plotted in decibel [dB] scale using a reference velocity $v_o = 5\text{e}{-8}$ m/s [7]. The response of the top layer is shown in Fig. 5, which compares well with the results presented in Ref. [6,7] for similar structures. As discussed in Ref. [7], the response can be divided into frequency zones. In the low-frequency range, the response of the beam can be approximated by that of an equivalent homogeneous panel whose properties can be determined through the application of basic structural mechanics relations applied to the unit cell elements [18,19], or through energy considerations [20]. This frequency range is limited by the intracell resonance, i.e., when wavelengths become of the order of the length of the core elements. Above these frequencies, equivalent homogenization fails, as discussed extensively in Refs. [19,20], and methods such as the spectral formulation here described need to employed. Fig. 5 shows that after the first few fundamental resonances of the panel, the response tends to a minimum value, after which it increases again to reach peaks at approximately 2600 and 3700 Hz. The deformed configurations of the beam in the different frequency zones are depicted in Fig. 6, which demonstrates the fundamental difference in the beam's behavior as frequency increases. For low-frequency values, the beam undergoes bending deformations similar to those occurring for a uniform beam. At frequencies around 2400 Hz, the deformation of the

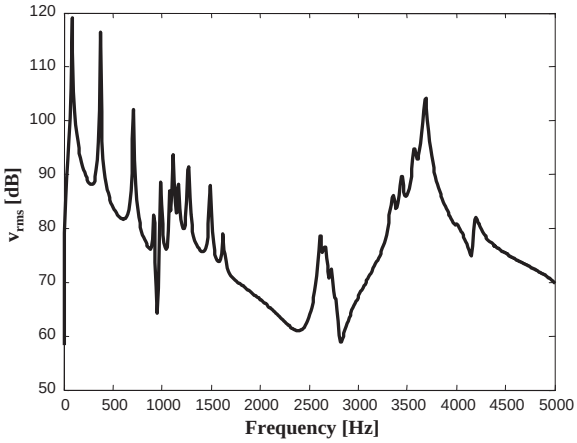

Fig. 5. Root mean velocity for the top layer of the square core beam.

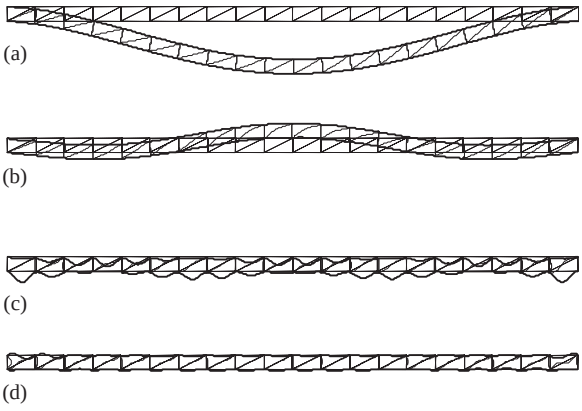

Fig. 6. Examples of deformed configurations for the square core beam. (a) $f = 80$ Hz, (b) 370 Hz, (c) 2400 Hz and (d) 3700 Hz.

core elements becomes comparable with those of the constraining layers. The deformation of the core is responsible for the attenuation of the beam response at these frequencies. As the frequency increases, the deformation is again mostly localized in the top and bottom layers, while the core remains almost undeformed. The peak occurring at approximately 3700 Hz represents an important limiting factor for the acoustic insulation capabilities of the considered class of beams, as a maximum in the structural response is likely to correspond to a minimum in sound transmission loss.

5.2.3. *Unit cell analysis*

The analysis of the beam response characteristics in the high-frequency range requires an accurate evaluation of the deformation patterns of each unit cell of the assembly. A separate analysis is carried out by considering a structure composed of a single cell. This elementary structure is again excited on its top layer by a uniform pressure of unit amplitude. The nodes at the cell boundaries are constrained in rotation, but left free to translate in the x and y directions. This particular configuration has been selected as the one providing the closest conditions encountered by the cell when assembled with the rest of the structure. The root mean square velocity of the top layer of the unit cell is shown in Fig. 7. The plot shows three main peaks at approximately 1120, 2600 and 3700 Hz. The peak at 2600 Hz is followed by an antiresonance at approximately 2700 Hz, which corresponds to the antiresonance predicted for the whole structure (see Fig. 5). All the four peaks also appear in the response of the complete beam. The considered analysis for the unit cell hence provides useful indications for the design of the considered class of beams, and can be used to predict the frequency values where the internal resonance of the cell affects the overall beam response. The deformed configuration of the cell at 1120, 2600, 2700 and 3700 Hz are shown in Fig. 8, which indicate the different behavior of the cell at these frequency values. In the antiresonance region, deformations are mainly localized in the core, while at 1120, 2600 and 3700 Hz the top and bottom layer are mostly bending, while the core remains almost undeformed.

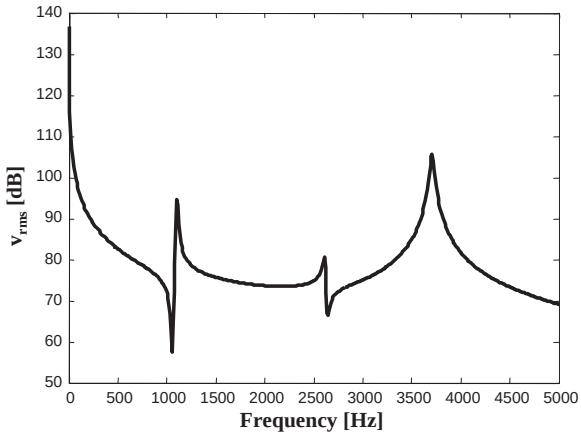

Fig. 7. Root mean velocity for the top layer of a unit square cell.

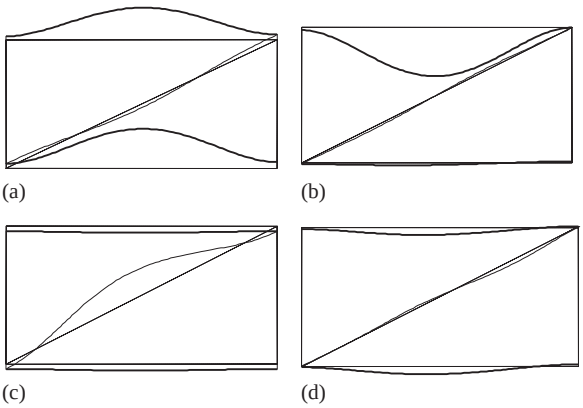

Fig. 8. Unit cell analysis: deformed configurations at resonance and antiresonance frequencies. (a) $f = 1120$ Hz, (b) 2600 Hz, (c) 2700 Hz and (d) 3700 Hz.

5.2.4. *Influence of core geometry*

The influence of the core geometry on the vibration response of the beam is also investigated. The analysis is carried out by keeping the overall dimensions of the beam, as well as the dimensions of each cell constant. The parameter that is allowed to change is the thickness of the core elements, to estimate the sensitivity of the overall performance of the beam. Thickness values of 1.25, 2.5 and 5 mm are considered, and both unit cell and complete beam response are computed for each thickness value. The results are presented in Fig. 9, which shows that changing the thickness slightly modifies the location of the antiresonance region as well as the resonance peaks. The plots of Fig. 9 also confirm the validity of the unit cell analysis as a tool to predict the main characteristics of the overall response. Finally, the results indicate that changing the thickness of the core only moderately modifies the response characteristics of the beam. The limited sensitivity of the beam's response with respect to the thickness of the core elements

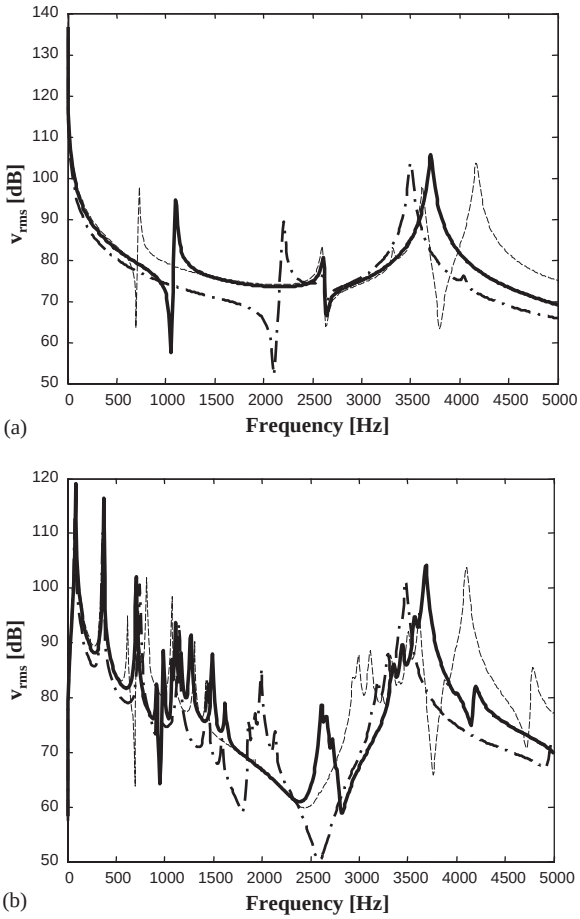

Fig. 9. Influence of core element thickness: (a) response of the unit cell analysis and (b) of the complete beam. (—·—, $h_c = 1.25$ mm; ——, $h_c = 2.5$ mm; - - - -, $h_c = 5$ mm).

motivates the effort of searching for alternative core topologies, which increase the design flexibility for the considered truss core beams.

5.3. Structural response of hexagonal core beams

The effect of the core internal angle is evaluated for constant dimensions of the unit cell and of the beam. The goal is to substantially modify the beam response characteristics without altering its external dimensions (length and thickness). To this end, the internal angle is varied between -30° and 30°, and the effect of such a change on the beam response is investigated.

The same dimensions and material properties used for the analysis of the square core configurations are here considered. The beams are again connected to the rigid baffle by pin joints, thus simulating simply supported boundary conditions.

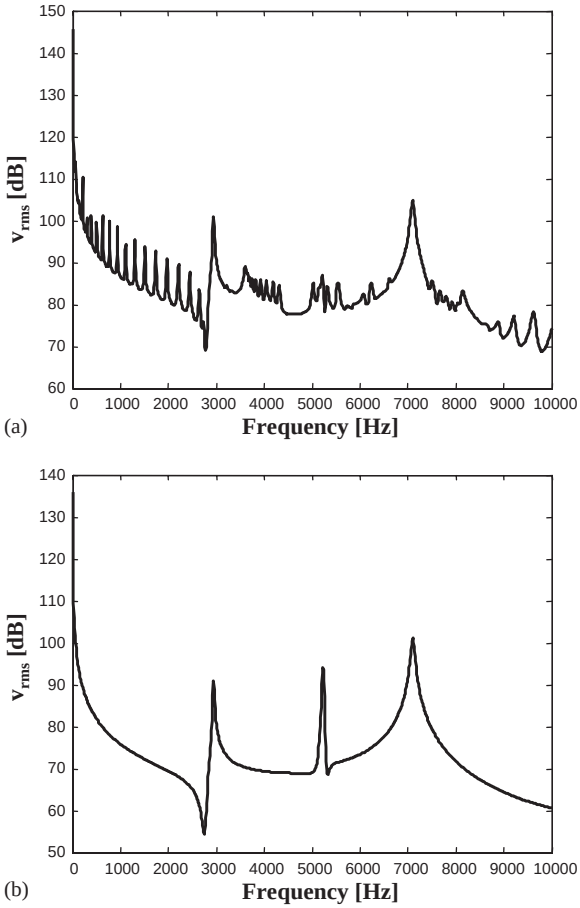

Fig. 10. Hexagonal core beam with $\theta = -30^\circ$: (a) response of top layer of the complete beam, and (b) of the unit cell.

5.3.1. Unit cell and beam response

The response of a beam composed of cells with internal angle $\theta = -30^\circ$ is shown in Fig. 10(a), while Fig. 10(b) presents the response predicted through the unit cell analysis. The frequency range of investigation is here extended to the 0–10,000 Hz range, to include some important features of the deformation for the hexagonal core beams. The unit cell obtained with this value of the internal angle undergoes three resonances in the considered range, which occur approximately at 2950, 5225 and 7100 Hz. Peaks corresponding to these resonance frequencies can be clearly noticed in the response of the complete beam, those at 2950 and 7100 Hz in particular. In addition, an antiresonance condition immediately precedes the first peak. As compared to the square cells, the hexagonal cell resonates at significantly higher frequencies, which causes the most significant peaks in the response of the complete beam to be shifted towards correspondingly higher frequency values. These peaks, as discussed in the following section, are responsible for high acoustic radiation. Shifting the cell internal resonance thus extends the frequency range within which the considered class of beams operates as efficient sound isolators. The radiation

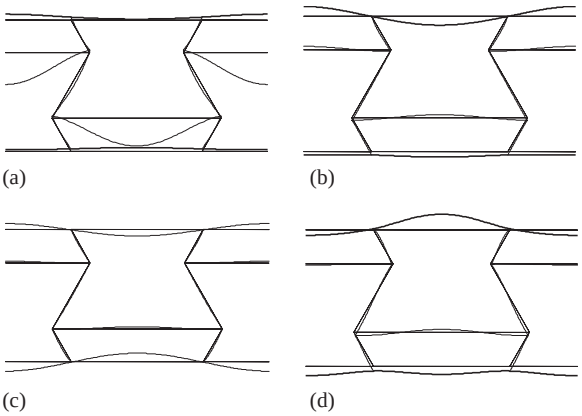

Fig. 11. Unit cell analysis for $\theta = -30^\circ$ hexagonal core: deformed configurations at resonance and antiresonance frequencies. (a) $f = 2850$ Hz, (b) 2950 Hz, (c) 5225 Hz and (d) 7100 Hz.

efficiency of the beams corresponding to the internal resonance of the cells can be better understood from the analysis of the cell deformed configurations at the resonance frequencies shown in Fig. 11. At 2950, 8225 and 7100 Hz, the deformation is mostly concentrated in the top and bottom layers, which also tend to vibrate out-of-phase with respect to each other. This out of phase behavior is particularly evident at 5225 and 7100 Hz. The condition of antiresonance at 2850 Hz again corresponds to deformations mostly localized in the core elements.

The influence of the cell internal angle on the unit cell and complete beam response is shown in Figs. 12 and 13, which respectively compare the behavior of beams with internal angles equal to $\pm 30^\circ$ and $\pm 10^\circ$. The plots demonstrate how the internal angle significantly affects the location of the internal resonance of the cell. Such significant change can be achieved without modifying the material, the cell dimensions or the thickness of the core elements, and demonstrate the design flexibility provided by the hexagonal core configurations.

With respect to the square core beams, the hexagonal configuration shows higher modal density and lower fundamental bending frequencies, which may indicate a lower static stiffness or load carrying capacity at low frequencies. Higher modal density and lower fundamental frequencies are also associated to the higher mass of the honeycomb configurations. The comparison of the static performance and the analysis of the mechanical characteristics of hexagonal truss core beams should complement the high-frequency vibro-acoustic characterization performed in this work and should therefore be the object of future investigations.

5.4. Sound radiation and sound radiation index

The fluid in contact with the top layer is air ($\rho_f = 1.2\,\mathrm{kg/m^3}$, $c_a = 343\,\mathrm{m/s}$). The beams are excited by plane pressure waves as described by Eq. (21) incident on the bottom layer according to the configuration depicted in Fig. 3. Normally incident waves ($\alpha = 0$) of unit amplitude ($p_{io} = 1\,\mathrm{Pa}$) and frequency ω varying between 0 and 5000 Hz are here considered.

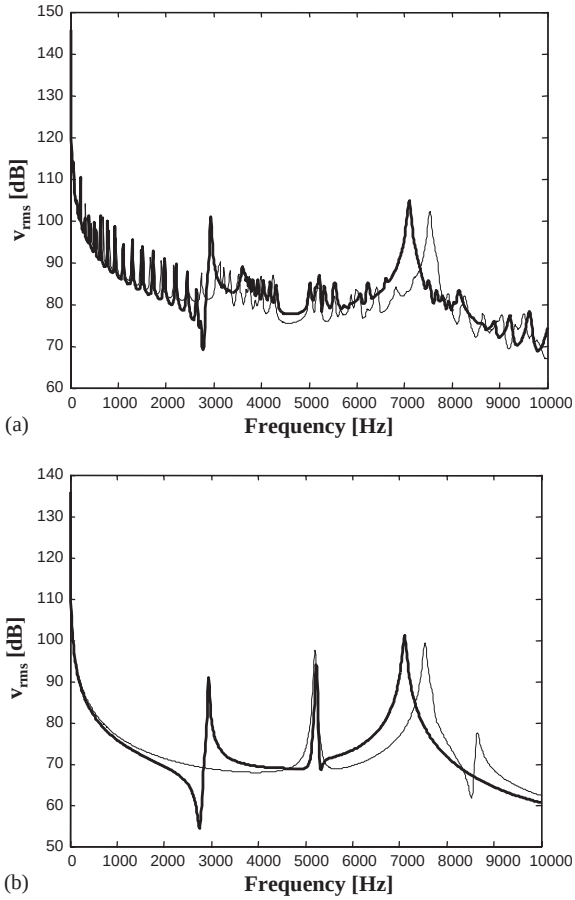

Fig. 12. Influence of internal angle: (a) response of the complete beam and (b) of the unit cell (b) (——, $\theta = -30°$; ——, $\theta = 30°$).

5.5. Sound radiation and sound transmission loss

The acoustic performance of the considered class of structures and their potential application for acoustic transmission reduction is investigated through the evaluation of the sound transmission loss (STL) and by evaluating the sound radiation in the acoustic domain interacting with the top layer of the beam. The sound transmission loss (STL) is defined as

$$\mathrm{STL} = 10 \log_{10}\left(\frac{1}{\tau_s}\right), \tag{35}$$

where the sound transmission coefficient τ_s is given by the ratio of the transmitted to the incident sound intensity [17] and can be expressed as

$$\tau_s = \frac{\int_0^L \mathrm{i}\omega p_t(x,0,\omega) w_t^*(x,\omega)\,\mathrm{d}x}{\int_0^L \mathrm{i}\omega p_i(x,0,\omega) w_b^*(x,\omega)\,\mathrm{d}x}. \tag{36}$$

In Eq. (36), p_t and p_i are the incident and transmitted sound pressures defined in Section 4.

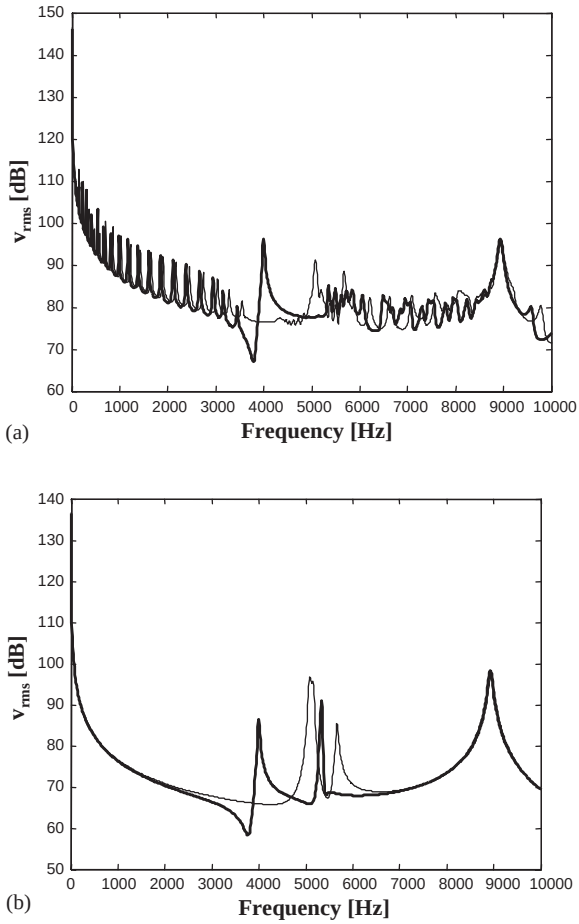

Fig. 13. Influence of internal angle: (a) response of the complete beam and (b) of the unit cell (——, $\theta = -10^\circ$; ——, $\theta = 10^\circ$).

The STLs for beams with hexagonal core are compared with that of the square core beam in Figs. 14 and 15. The plots confirm the indications obtained from the analysis of the structural response of the beams discussed in Section 5.3. The sound transmission reduction capabilities of the square core beam are significantly reduced at frequencies corresponding to the internal resonance of the cells, i.e., 1120, 2600 and 3700 Hz. The maximum STL is achieved before the 2600 Hz resonance and at frequencies corresponding to the antiresonance at 2700 Hz, where a narrow peak can be observed. The hexagonal beams overall perform better than the square core beam, as their efficiency is extended to the complete frequency range in consideration, and the internal resonances have a lesser effect on the STLs. The performance of beams with internal angle $\theta = \pm 10^\circ$ is particularly noteworthy, as the STL does not decay and remains always higher than that of the square core beams in the considered frequency range. Such a behavior can be justified by observing that the configurations for $\theta = \pm 10^\circ$ have the highest frequency of internal resonance, as shown in Fig. 13. Finally, one can also note that negative internal angles overall

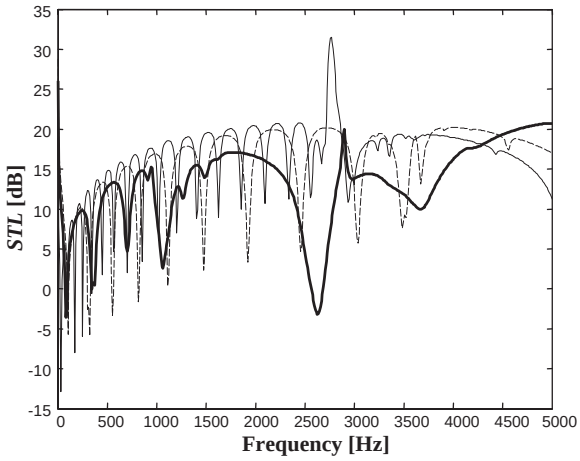

Fig. 14. STL for square and hexagonal core beams (——, square; ——, $\theta = -30^\circ$; - - - -, $\theta = 30^\circ$).

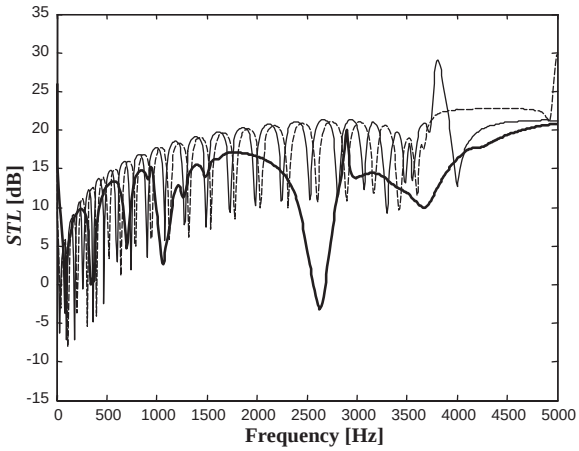

Fig. 15. STL for square and hexagonal core beams: (——, square; ——, $\theta = -10^\circ$; - - - -, $\theta = 10^\circ$).

seem to provide higher STLs over most of the considered frequency range than the configuration with $\theta > 0$.

The core topology influences the dynamic behavior of the sandwich beams and modifies their sound radiation pattern. In order to visualize and evaluate the influence of the core on the sound radiation characteristics of the considered beams, the pressure radiated in the acoustic domain is determined through the procedure outlined in Section 4. Sound pressure distributions for the considered beams are plotted and compared. The radiated pressure is presented in the form of sound pressure level (SPL), calculated according to the standard formula [21]

$$\mathrm{SPL}(x, y, \omega) = 20 \log_{10}\left(\frac{p_t(x, y, \omega)}{p_{ref}}\right), \tag{37}$$

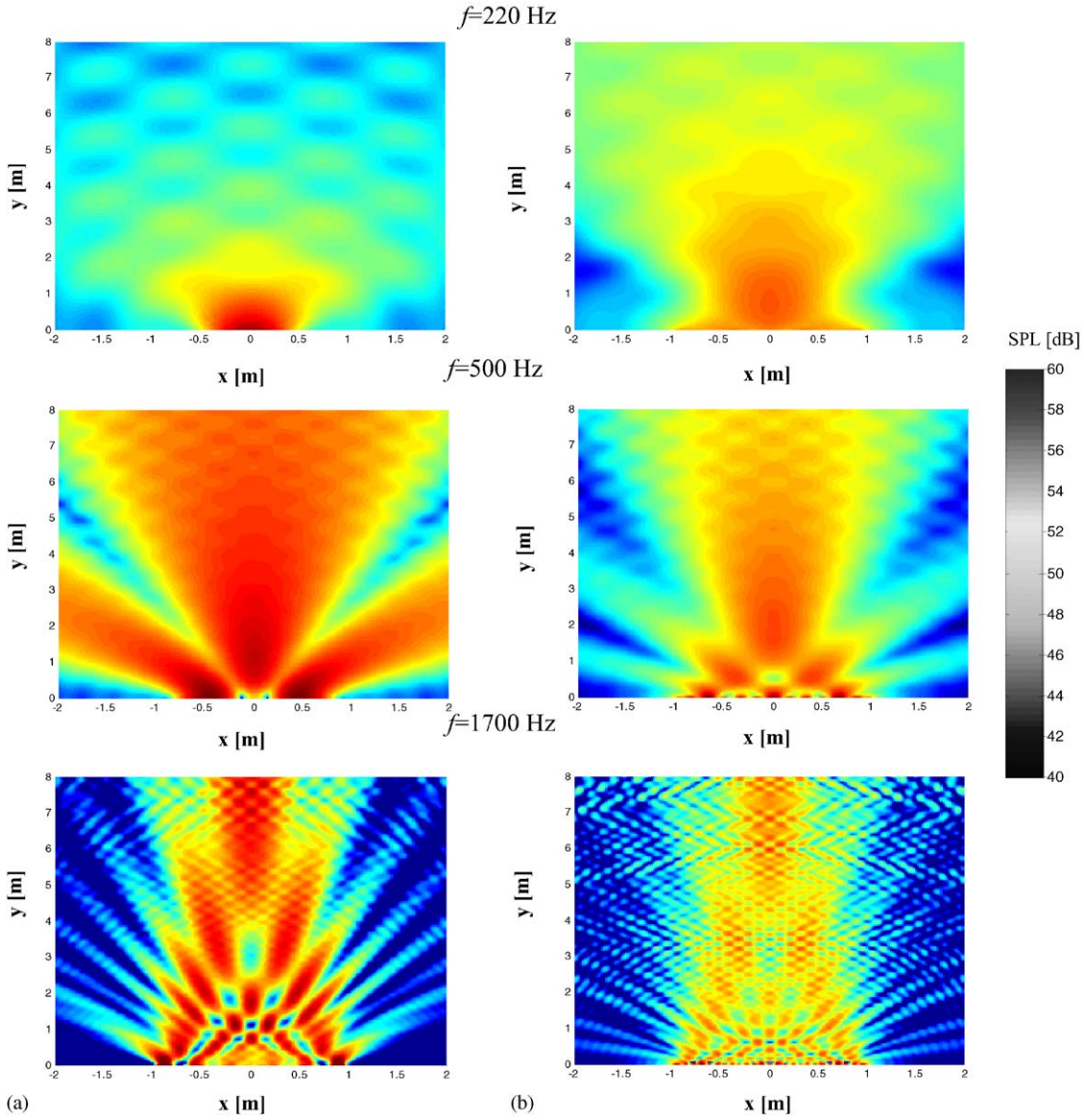

Fig. 16. Radiated sound pressure levels (SPLs) for (a) square and (b) hexagonal core beams.

where p_{ref} is the reference pressure, which in air is taken equal to 20 μPa. Using this reference value, the SPL corresponding to the amplitude of the incident pressure on the bottom layer, taken equal to 1 Pa, is approximately 94 dB.

Examples of SPL distributions are shown in Fig. 16, where comparisons between square and honeycomb core with $\theta = -30^\circ$ are made for frequency of the incident pressure wave equal to 220, 500 and 1700 Hz. These values of frequency are chosen as representative of the low, middle and high-frequency behavior of the considered structures. In the maps, the beams are located

between $x = -1$ m and $x = 1$ m, at $y = 0$. The radiated SPLs by the honeycomb core beam are always lower than that of the square core beam, and the attenuation increases with frequency.

6. Conclusions

This paper analyzes the vibration and acoustic performance of sandwich beams with honeycomb core. The honeycomb geometry is arranged through the thickness as opposed to conventional sandwich honeycomb constructions. The proposed configurations represent an alternative to previously proposed truss core and prismatic material designs. Particular focus is placed on evaluating the influence of the core geometry and shape on the dynamic structural response and on the sound radiation of the considered class of beams. The analysis is performed for hexagonal and re-entrant topologies, with a square truss core used as baseline for comparison.

A finite element is developed to predict the dynamic response of the sandwich beam. The formulation uses dynamic shape functions, which allow for accurate predictions of the structure's dynamic behavior with a reduced number of elements and within a wide frequency range. The formulation is also coupled with a FT based analysis of the sound radiation in a semi-infinite acoustic domain interacting with one side of the structure.

The performance of beams with various core configurations is evaluated and compared in terms of structural response and sound radiation. The structural analysis shows that the beam response is characterized by attenuation zones, which are defined by the internal resonance of the core elements. A unit cell analysis is also presented to investigate the effect of its resonance on the overall response of the structure. The presented results indicate that unit cell resonances show up also in the response of the complete beam. The considered analysis of the unit cell hence allows predicting the characteristics of the assembled beam and can be thus used as an effective design tool. The comparison between square core beams and hexagonal configurations indicates that the latter undergo cell resonances at higher frequency and hence behave as efficient isolators over a wider frequency range. This behavior is confirmed by the evaluation of the STL, when the beams are used as partitions between fluid domains.

The results presented in this paper suggest the potential advantages of a truss core with honeycomb topology and indicate that re-entrant configurations are generally more effective for vibration and sound transmission reduction applications. The presented results focus only on the assessment of the influence of the core internal angle, for a fixed number of cells along the length of the beam and across its thickness. Further studies should be performed to investigate the effect of the cell dimensions and to investigate the performance of other alternative layouts. The analysis should be then extended to plates with three-dimensional truss cores, and should address the optimization of their static load carrying characteristics in conjunction with the structural-acoustic behavior. Finally, the developed numerical model should be validated experimentally.

Acknowledgements

The author wishes to thank the National Science Foundation for the support provided for this work under the grant CMS-0201371.

References

[1] L.J. Gibson, M.F. Ashby, *Cellular Solids*: *Structure and Properties*, 2nd Edition, Cambridge University Press, Cambridge, UK, 1997.

[2] A.G. Evans, J.W. Hutchinson, N.A. Fleck, M.F. Ashby, H.N.G. Wadley, The topological design of multifunctional cellular metals, *Progress in Materials Science* 46 (2001) 309–327.

[3] M.F. Ashby, A.G. Evans, N.A. Fleck, L.J. Gibson, J.W. Hutchinson, H.N.G. Wadley, *Metal Foams*: *A Design Guide*, Butterworth-Heinemann, London, 2000.

[4] J.C. Wallach, L.J. Gibson, Mechanical behavior of a three-dimensional truss material, *International Journal of Solids and Structures* 38 (2001) 7181–7196.

[5] N. Wicks, J.W. Hutchinson, Optimal truss plates, *International Journal of Solids and Structures* 38 (2001) 5165–5183.

[6] M. El-Raheb, Frequency response of a two-dimensional trusslike periodic panel, *Journal of the Acoustical Society of America* 101 (6) (1997) 3457–3465.

[7] M. El-Raheb, P. Wagner, Transmission of sound across a trusslike periodic panel: 2d analysis, *Journal of the Acoustical Society of America* 102 (4) (1997) 2176–2183.

[8] M. El-Raheb, P. Wagner, Effects of end cap and aspect ratio on transmission of sound across a truss-like periodic double panel, *Journal of Sound and Vibrations* 250 (2) (2002) 299–322.

[9] F. Scarpa, G. Tomlinson, Theoretical characteristics of the vibration of sandwich plates with in-plane negative Poisson's ratio values, *Journal of Sound and Vibrations* 230 (1) (2000) 45–67.

[10] C.T. Herakovich, Composite laminates with negative through-the-thickness Poisson's ratios, *Journal of Composite Materials* 18 (1984) 447–455.

[11] K.E. Evans, Design of doubly curved sandwich panels with honeycomb cores, *Computers and Structures* 17 (2) (1991) 95–111.

[12] M. Ruzzene, F. Soranna, F. Scarpa, Wave beaming effects in bi-dimensional cellular structures, *Smart Materials and Structures* 12 (3) (2003) 363–372.

[13] J.F. Doyle, *Wave Propagation in Structures*, 2nd Edition, Springer, New York, 1997.

[14] J.F. Doyle, A spectrally formulated finite element for longitudinal wave propagation, *International Journal of Analytical and Experimental Modal Analysis* 3 (1988) 1–5.

[15] S. Gopalakrishnan, J.F. Doyle, Wave propagation in connected wave guides of varying cross section, *Journal of Sound and Vibration* 175 (3) (1994) 347–363.

[16] M.C. Junger, D. Feit, *Sound, Structures and Their Interaction*, 2nd Edition, The Acoustical Society of America, 1993.

[17] F. Fahy, *Sound and Structural Vibration*: *Radiation, Transmission and Response*, Academic Press, New York, 1985.

[18] T.S. Lok, Q.H. Cheng, Free vibration of clamped orthotropic sandwich panel, *Journal of Sound and Vibration* 229 (2) (2000) 311–327.

[19] A.K. Noor, Continuum modeling for repetitive lattice structures, *Applied Mechanics Reviews* 41 (7) (1988) 285–296.

[20] U. Lee, Equivalent continuum models of large platelike lattice structures, *International Journal of Solids and Structures* 31 (4) (1994) 457–467.

[21] L.E. Kinsler, A.R. Frey, A.B. Coppens, J.V. Sanders, *Fundamentals of Acoustics*, 4th Edition, Wiley, New York, 2000.